High-Resolution Smoke Forecasting for the 2018 Camp Fire in California

Fotini Katopodes Chow, Katelyn A. Yu, Alexander Young, Eric James, Georg A. Grell, Ivan Csiszar, Marina Tsidulko, Saulo Freitas, Gabriel Pereira, Louis Giglio, Mariel D. Friberg, and Ravan Ahmadov

ABSTRACT: Smoke from the 2018 Camp Fire in Northern California blanketed a large part of the region for 2 weeks, creating poor air quality in the "unhealthy" range for millions of people. The NOAA Global System Laboratory's HRRR-Smoke model was operating experimentally in real time during the Camp Fire. Here, output from the HRRR-Smoke model is compared to surface observations of $PM_{2.5}$ from AQS and PurpleAir sensors as well as satellite observation data. The HRRR-Smoke model at 3-km resolution successfully simulated the evolution of the plume during the initial phase of the fire (8–10 November 2018). Stereoscopic satellite plume height retrievals were used to compare with model output (for the first time, to the authors' knowledge), showing that HRRR-Smoke is able to represent the complex 3D distribution of the smoke plume over complex terrain. On 15–16 November, HRRR-Smoke was able to capture the intensification of $PM_{2.5}$ pollution due to a high pressure system and subsidence that trapped smoke close to the surface; however, HRRR-Smoke later underpredicted $PM_{2.5}$ levels due to likely underestimates of the fire radiative power (FRP) derived from satellite observations. The intensity of the Camp Fire smoke event and the resulting pollution during the stagnation episodes make it an excellent test case for HRRR-Smoke in predicting $PM_{2.5}$ levels, which were so high from this single fire event that the usual anthropogenic pollution sources became insignificant. The HRRR-Smoke model was implemented operationally at NOAA/NCEP in December 2020, now providing essential support for smoke forecasting as the impact of U.S. wildfires continues to increase in scope and magnitude.

KEYWORDS: Dispersion; Numerical weather prediction/forecasting; Aerosols/particulates; Air quality; Forest fires; Wildfires

AFFILIATIONS: Chow, Yu, and Young*—Civil and Environmental Engineering, University of California, Berkeley, Berkeley, California; **James and Ahmadov**—CIRES, University of Colorado Boulder, and NOAA Global Systems Laboratory, Boulder, Colorado; **Grell**—NOAA Global Systems Laboratory, Boulder, Colorado; **Csiszar**—Center for Satellite Applications and Research, NOAA National Environmental Satellite, Data, and Information Service, College Park, Maryland; **Tsidulko**—I.M. Systems Group, Rockville, Maryland; **Freitas***—Universities Space Research Association, Columbia, and Global Modeling and Assimilation Office, NASA GSFC, Greenbelt, Maryland; **Pereira**—Department of Geosciences, Federal University of São João del-Rei, São João del-Rei, Brazil; **Giglio**—Geographical Sciences, University of Maryland, College Park, College Park, Maryland; **Friberg**—NASA GSFC, University of Maryland, College Park, College Park, Maryland
*CURRENT AFFILIATIONS: Young—Cornell University, Ithaca, New York; **Freitas**—National Institute for Space Research, São José dos Campos, Brazil

Major wildfire events have increasingly intersected with urban communities in recent years. Apart from wildfires crossing the wildland–urban interface, wildfire smoke can affect communities hundreds of miles away. The Camp Fire, which started on 8 November 2018 near Paradise, California, is a prime example of an event that had inordinate effects on regional air quality and visibility. The Camp Fire destroyed almost 19,000 structures, killed 88 people (California's deadliest fire to date), and displaced over 50,000 people from their homes (Ban et al. 2020; Palinkas 2020). In addition, millions of people in Northern California were exposed to poor air quality for many days, with potential health impacts including increased mortality and other health complications (Palinkas 2020; Balmes 2020; Holm et al. 2021; Reid et al. 2016; Wettstein et al. 2018; Liu et al. 2017; Li et al. 2020; Burke et al. 2021). Similarly, multiweek air quality impacts were seen during the 2020 fire season due to numerous large wildfires throughout the western United States (Rooney et al. 2020; Mass and Ovens 2021).

Air quality forecast guidance is typically produced in a partnership of federal and local agencies and disseminated through airnow.gov and other websites. During the Camp Fire in 2018, this website was inundated with traffic, rendered unavailable (Knobel 2018), and could only report very coarse spatial patterns in the estimated air quality index (AQI) based on sparsely distributed air quality sensors. The smoke from the Camp Fire reached the San Francisco Bay Area, with a population of about 8 million people, within hours of fire ignition. The smoke persisted for about 2 weeks, in many places intensifying during the middle of this period due to a high pressure system with subsidence and shallow mixing-layer heights. On 10 November 2018 (the third day of the Camp Fire), $PM_{2.5}$ levels reached "unhealthy" levels (151–200 AQI) for the whole Bay Area. On 16–18 November, Bay Area air quality worsened further, reported to be among the worst in the world, with the AQI reaching higher than 250 in San Francisco ($>200\ \mu g\ m^{-3}$), prompting widespread school closures and flight cancellations (Mass and Ovens 2021).

High-resolution smoke forecasts are needed to provide reliable spatial and temporal information during extreme wildfire events. NOAA has been running the High-Resolution Rapid Refresh (HRRR) model at 3-km grid spacing to provide hourly convection-permitting weather forecasts over the entire continental United States (Benjamin et al. 2016). Since its operational implementation in 2014, the HRRR has become an essential tool for weather forecasters. It is widely used for predicting hazardous weather in applications ranging from severe thunderstorms and heavy rainfall to low cloud ceilings and reduced visibility

(see, e.g., Benjamin et al. 2021). In 2016, a single smoke tracer (primary $PM_{2.5}$), a plume rise parameterization (Freitas et al. 2007, 2010), and satellite fire radiative power (FRP) processing (Ahmadov et al. 2017) were implemented in an experimental version of the HRRR model, referred to as the HRRR-Smoke model. Fire radiative power (measured in watts) is the rate of radiative energy emitted by the fire, and is used to prescribe smoke surface fluxes in the model. During the Camp Fire event, HRRR-Smoke was operated in real-time demonstration mode by the NOAA Global Systems Laboratory (GSL) with graphical forecast output available online (https://rapidrefresh.noaa.gov/hrrr/HRRRsmoke/). The HRRR-Smoke model became fully operational at NOAA/NCEP in December 2020.

Here we examine the ability of the HRRR-Smoke model to capture the smoke plumes generated by the 2018 Camp Fire to produce $PM_{2.5}$ forecasts for affected communities. The HRRR-Smoke model has recently been evaluated in a model intercomparison study for the 2019 Williams Flats fire (Ye et al. 2021). For the present study, the model has been rerun for the Camp Fire case using a more recent version of the code (HRRRv4, implemented operationally in December 2020) to better evaluate its forecasting abilities for such an exceptional air quality event. Model outputs are compared to data from the AQS and PurpleAir community air quality sensors (see appendix), meteorological station data, and satellite observations.

This paper presents the first in-depth analysis of the ability of the HRRR-Smoke coupled weather–smoke model to provide smoke forecasting at 3-km resolution, which is a major milestone for a model with a domain of this size (covering the continental United States). The coupled modeling framework and hourly refresh cycle make HRRR-Smoke a powerful tool for forecasting such extreme smoke pollution events. The Camp Fire is an excellent case study due to the relatively clean background air (no other major wildfires in the western United States) and the very high concentrations of smoke, which persisted over the region for an extended time period. The Camp Fire occurred during November, also making this a unique smoke event compared to summertime, when multiple wildfires typically affect air quality across urban areas in the western United States and multiday stagnation events typically do not occur. Combined with a dense network of sensors (AQS and PurpleAir), this study of the 2018 Camp Fire also provides an opportunity to envision a more accurate forecast system that could ultimately be combined with real-time data to give communities better predictions during smoke events.

A number of other studies have presented research simulations of the Camp Fire event. Rooney et al. (2020) describe WRF-Chem simulations of the event, demonstrating reasonable performance for surface $PM_{2.5}$, and plume height as verified against Tropospheric Monitoring Instrument (TROPOMI) observations. Mass and Ovens (2021) describe nested WRF simulations of the meteorology associated with the first day of the Camp Fire, showing accurate forecasts of the downslope windstorm contributing to rapid fire spread. Brewer and Clements (2020) describe additional high-resolution WRF simulations of the meteorological evolution. Li et al. (2020) present ensemble HYSPLIT simulations of surface $PM_{2.5}$ during the Camp Fire event, documenting a very large ensemble spread due to variations in plume rise, meteorological input, emissions datasets, and model configuration.

The National Weather Service report after the Camp Fire recommended "a consistent source of smoke transport model guidance (e.g., HRRR-Smoke)" to provide reliable forecasts and messaging (NWS Western Region Headquarters 2020). This model guidance will be particularly useful as the frequency of wildfire events near urban areas increases due to climate change (such as the fire incidents in the western United States in 2018–21) and for managing prescribed burns designed to prevent catastrophic wildfires (Miller et al. 2020). Improved forecasts, combined with dense networks of community-installed air quality sensors, will enable government agencies to give better guidance about smoke exposure to help protect disadvantaged communities and at-risk individuals and to more accurately

plan hospital emergency room demand. Predictions with increased spatial resolution can also help to provide more specific local guidance about limiting outdoor activities. In addition, weather prediction models can be improved by including smoke impacts on solar radiation reaching the surface; HRRR-Smoke has this capability (James et al. 2019; NESDIS 2021), but many operational weather prediction models do not, which can lead to significant forecast errors during intense smoke events. This feedback mechanism has been documented by the modeling studies of Grell et al. (2011) and Rooney et al. (2020), and the smoke impact on surface radiation was observed in measurements from the Camp Fire (Mass and Ovens 2021).

This paper begins with a description of the smoke plume evolution during the first few days of the Camp Fire event with comparisons to AQS and PurpleAir monitors at the surface and novel comparisons to stereoscopic satellite plume height data, followed by comparison with meteorological observations. The paper concludes with further comparison to satellite observations, including a discussion of model errors and future research areas related to satellite fire detection algorithms.

Spatial evolution of winds and smoke

Figure 1 shows the dramatic spread of wildfire smoke from the Camp Fire across Northern California, with snapshots of HRRR-Smoke $PM_{2.5}$ concentrations overlaid with wind vectors. Images are shown at 3-hourly intervals for 3–12 h after the fire was initialized in the model, at the surface and aloft. Details of the HRRR-Smoke model configuration are provided in the appendix. Near the ground, the east winds over the Sierras moved smoke into the Central Valley, where downvalley winds pushed the smoke southward toward the Bay Area. Aloft, the strong north-northeast winds drove the smoke across the Central Valley to the coastal mountain range. Continued north-northwest winds along the Central Valley created a V-shape in the near-surface smoke plume, as seen in Fig. 1.

The smoke prediction from HRRR-Smoke is dependent on the ingested satellite fire detections. The Camp Fire began around 1430 UTC 8 November 2018 (0630 local time) (NWS Western Region Headquarters 2020). The MODIS instrument on board the *Terra* satellite detected the fire about 4 h later at 1810 UTC (1010 local time). The HRRR-Smoke model therefore lags the observations by ~4–5 h on the day of the fire ignition, but is nevertheless able to capture the relative timing of the smoke arrival at different locations. Additionally ingesting geostationary satellite FRP data into the model could help to mitigate this detection delay issue in the future (O'Neill and Raffuse 2021), as described further in the "Satellite FRP detection challenges" section. As wildfires can start any time or evolve rapidly, it is important to ingest the satellite detections into the smoke forecast models with the shortest delay possible. Because new HRRR forecasts start every hour (rapid-update cycling) by assimilating the latest meteorological observations, this framework also allows ingesting the "latest" FRP detections into the model.

Figure 2 shows a snapshot of surface winds and smoke concentrations from HRRR-Smoke compared to surface $PM_{2.5}$ measurements from AQS and PurpleAir sensors. There is good qualitative agreement in the spatial structure of the plume observed by HRRR-Smoke and the collection of $PM_{2.5}$ sensors. Small errors in modeled wind speed and direction will affect the detailed shape of the modeled plume (see, e.g., Fig. 11 later), but there are large areas of agreement, despite the time delays mentioned above. The PurpleAir community-based sensors provide more spatially detailed $PM_{2.5}$ data with significantly less expensive sensors, and allow tracking of the smoke plume spatial variability, as seen, e.g., in the videos in the online supplemental material. The PurpleAir sensors have been validated in a few studies, e.g., Gupta et al. (2018), Delp and Singer (2020), and Barkjohn et al. (2021), which found that while the sensors are not as accurate as the quality-controlled AQS sensors, they
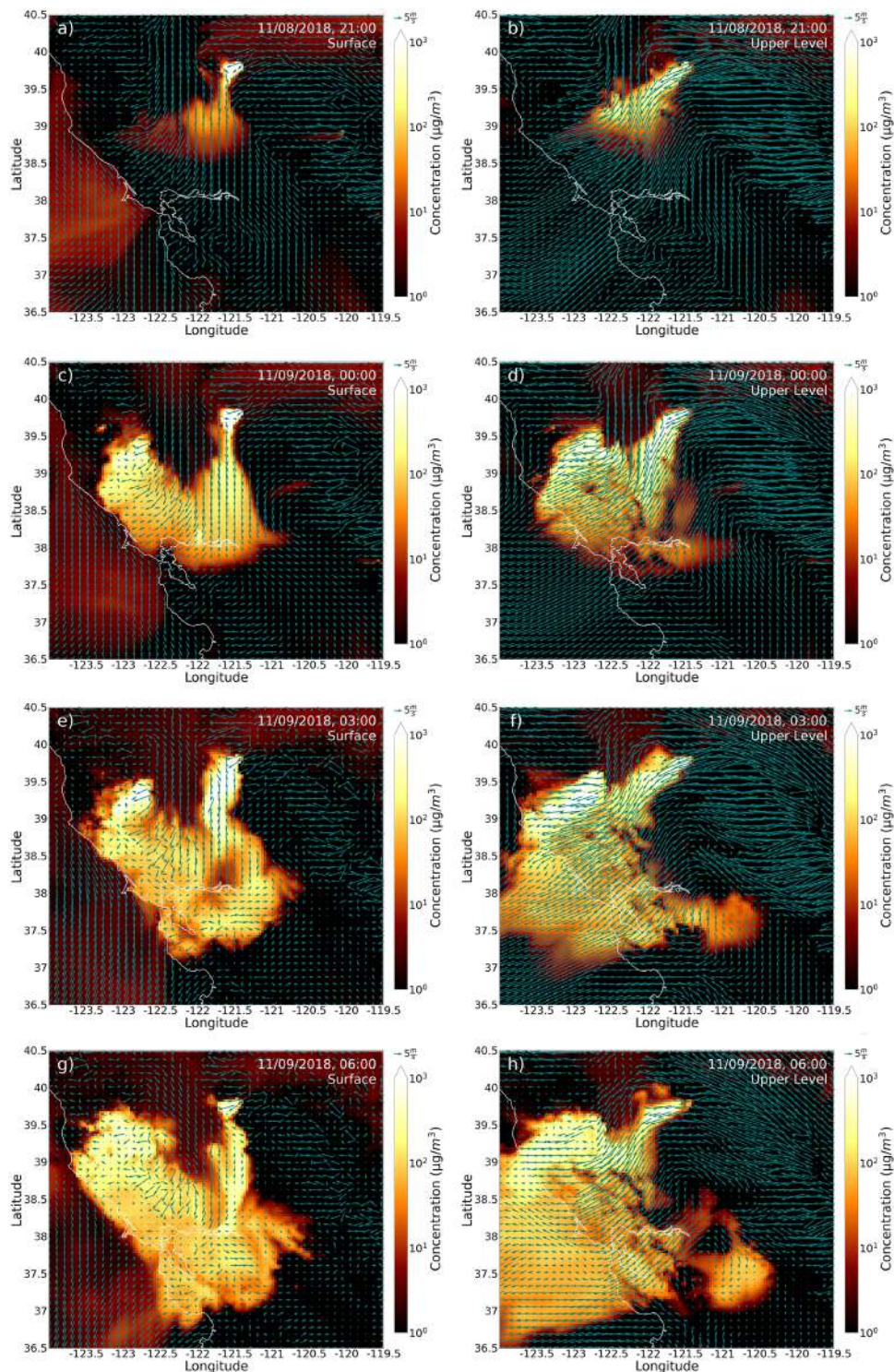
Fig. 1. Snapshot of (left) surface smoke ~8 and (right) 1829 m AGL smoke concentrations (PM$_{2.5}$, μg m^{-3}, contours on log scale) and wind vectors (cyan) from HRRR-Smoke every 3 h from 2100 UTC 8 Nov to 0900 UTC 9 Nov 2018 during the Camp Fire.

do capture trends and spatial variability. The PurpleAir data used here are adjusted by a factor of 0.48, following the analysis of Delp and Singer (2020), who compared PurpleAir with AQS sensors specifically during the 2018 Camp Fire event. The PurpleAir dataset was also filtered by removing indoor sensors and sensors with missing data as described in the appendix.

A more detailed comparison with surface observations for selected sensors (locations shown in Fig. 3) illustrates the ability of HRRR-Smoke to capture the smoke plume spread. Figure 4
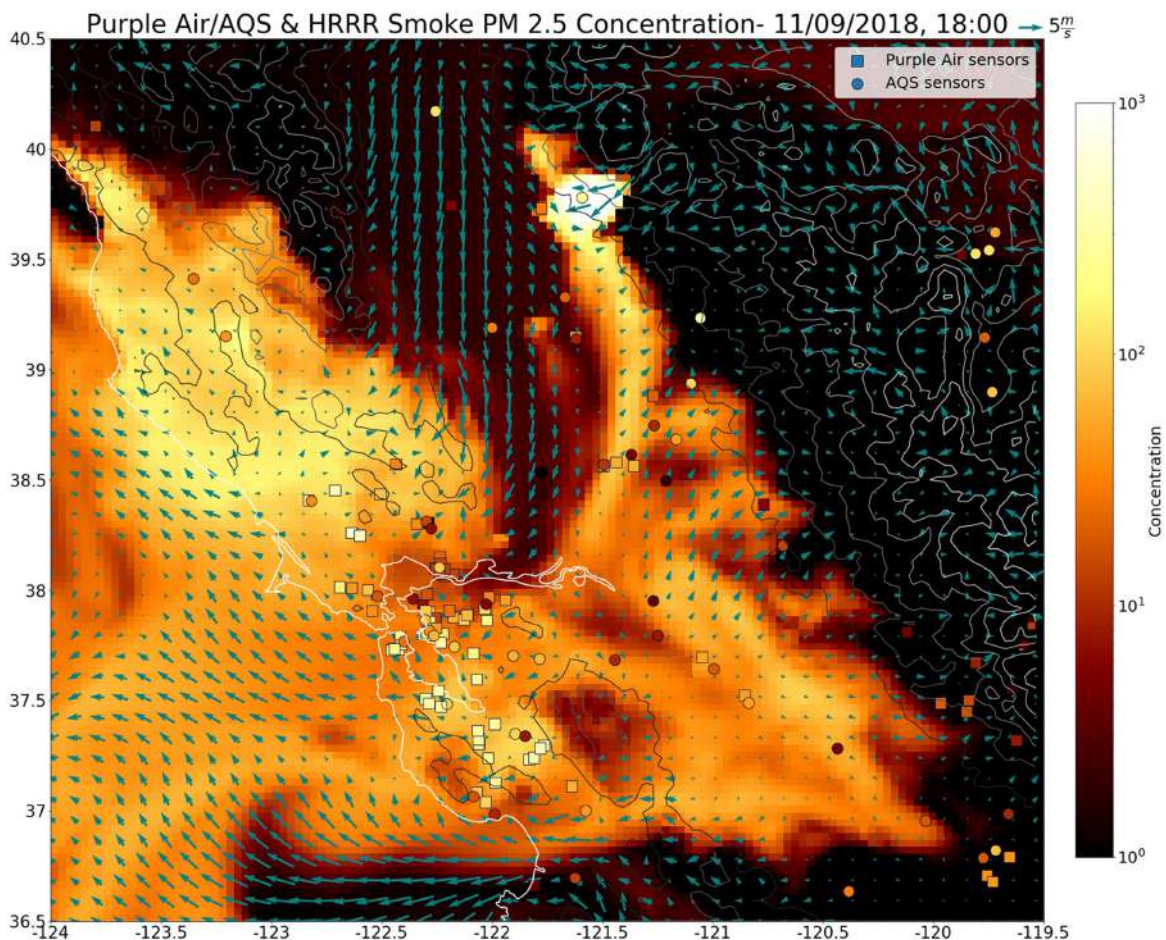
Fig. 2. Comparison of surface smoke concentrations (PM$_{2.5}$, μg m^{-3}) from HRRR-Smoke (contours) with PurpleAir (squares) and AQS (circles) stations at 1800 UTC 9 Nov. Surface wind vectors (cyan) also shown. Additional snapshots and a video are available in the supplemental material.

shows several time series of PM$_{2.5}$ concentrations at various distances along the main direction of the smoke plume: Sacramento (south of Paradise), East Bay (farther west), and South Bay (farther south). The PurpleAir sensors recorded ~1.6-h shifts in the arrival of the smoke plume at each subsequent location as measured by the time the 10 μg m^{-3} concentration threshold was crossed on 8 November 2018. These time shifts are seen by the HRRR-Smoke model as well, recording ~2.3 h shifts in the modeled plume arrival at the three designated sites, albeit delayed from the observations by 4.4, 5.1, and 5.8 h, respectively, due to late initiation of the fire and subsequent differences in meteorological forcing in the model at the later times. Comparisons between selected individual high-quality AQS sensors and HRRR-Smoke output in Fig. 5 show similar agreement between the model and the AQS observations, with data shown over the entire 2-week duration of the smoke event in the Bay Area, 8–21 November 2018. The shifted arrival times of the smoke plume are seen again here. The delay in the modeled smoke arrival time is also visible above in the contour plots of surface PM$_{2.5}$ concentration from HRRR-Smoke with PurpleAir and AQS sensors in Fig. 2, and in Fig. ES1 in the supplemental material. This delay is most apparent 3–24 h after the fire initialization in the model, where the sensors generally show higher values (brighter colors) in the earlier hours of the simulation, compared to HRRR-Smoke.

Further intensification of the smoke event during the second week illustrates the complex interaction of meteorology and emissions and points to the need for improved models and observations that can capture these details. After some initial improvement on days 3–6, there is a distinct worsening of air quality during days 7–9 of the event (14–16 November 2018).

The HRRR-Smoke model in general underpredicts concentrations during the second week, likely due to significant underestimations in the FRP data (see "Satellite FRP detection challenges" section). It appears that the reduction in smoke during the intermediate period from 11 to 14 November 2018 occurred because winds shifted to weak southerly, which pushed the smoke plume to the north. When winds shifted again to the north-northwest, the plume brought new smoke toward the Bay Area, which when combined with subsidence and a very stable capping inversion, led to very high near-surface concentrations of $PM_{2.5}$.

Fig. 3. RAWS, sounding, AQS, and PurpleAir data sampling locations used in this study. The Camp Fire was located near Paradise, CA. Cities of interest are marked in orange. Investigation areas are outlined with blue boxes.

This worsening of air quality prompted widespread school closures in the Bay Area with the highest-ever-recorded AQI values of 256 observed in Oakland (206 μg m^{-3}) and 271 in San Francisco (221 μg m^{-3}) on 16 November 2018 (Mass and Ovens 2021). HRRR-Smoke captures the sharp increase in $PM_{2.5}$ values at the start of this intensification period, though again with some delay, but greatly underpredicts smoke values for the duration of the Camp Fire smoke event.

Figure 6 shows a scatterplot of $PM_{2.5}$ daily averages (using local time) for the 53 AQS sensors located in the map area shown in Fig. 2 (only sensors without any missing data during this period were included). The color of each data point becomes lighter as a function of time, illustrating the underprediction of HRRR-Smoke during the second week of the smoke event (shown by the lighter red dot colors).

Model error statistics are computed for $PM_{2.5}$ daily averages from the HRRR-Smoke versus the AQS sensor data. Standard metrics for the HRRR-Smoke model daily averaged $PM_{2.5}$ compared to the 53 AQS sensors yield $r \sim 0.42$ ($r^2 \sim 0.17$), RMSE ~ 63.3 μg m^{-3}, and normalized mean error (NME) of 70.6%. These values are similar to those in the model intercomparison study of Ye et al. (2021), who report that all 13 of the models in their study of the Williams Flat fire showed $r < 0.35$ ($r^2 < 0.13$), RMSE > 9.8 μg m^{-3}, and NME $> 70\%$. Atmospheric dispersion model skill statistics are notoriously poor, and are difficult to compute and interpret because of small misalignments in wind direction and, hence, plume development, which can produce very large errors in the concentration field. For example, Fig. 4 shows a delay in the modeled arrival of the plume compared to observations, yet there is still predictive power in the simulations. For the Camp Fire event, the underprediction of HRRR-Smoke of the smoke intensification during the second week is evident by performing separate error calculations; errors from the first and second weeks of the event, shown in Table ES1 in the supplemental material, indicate an increase of RMSE from 44.05 in the first week to 80.01 in the second week, with a similar pattern in the other error metrics. It should also be noted that HRRR-Smoke does not include nonfire emission sources (e.g., anthropogenic) or gas/aerosol chemistry, hence the model cannot fully capture the observed $PM_{2.5}$.
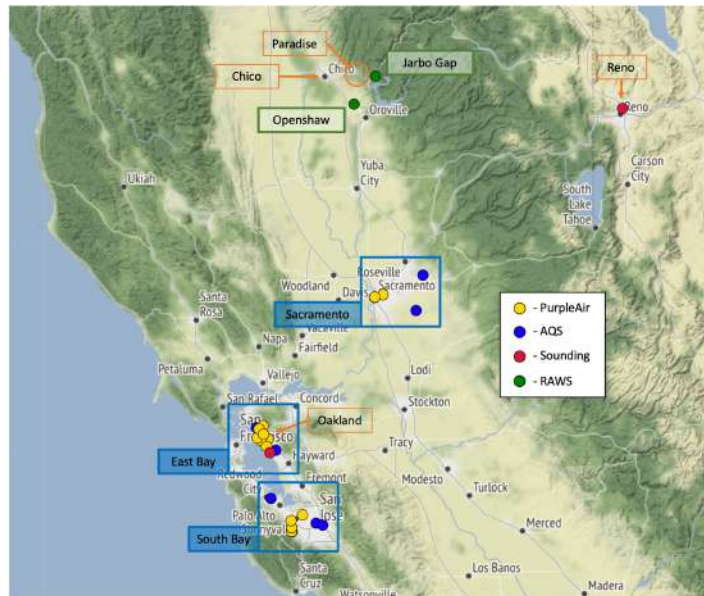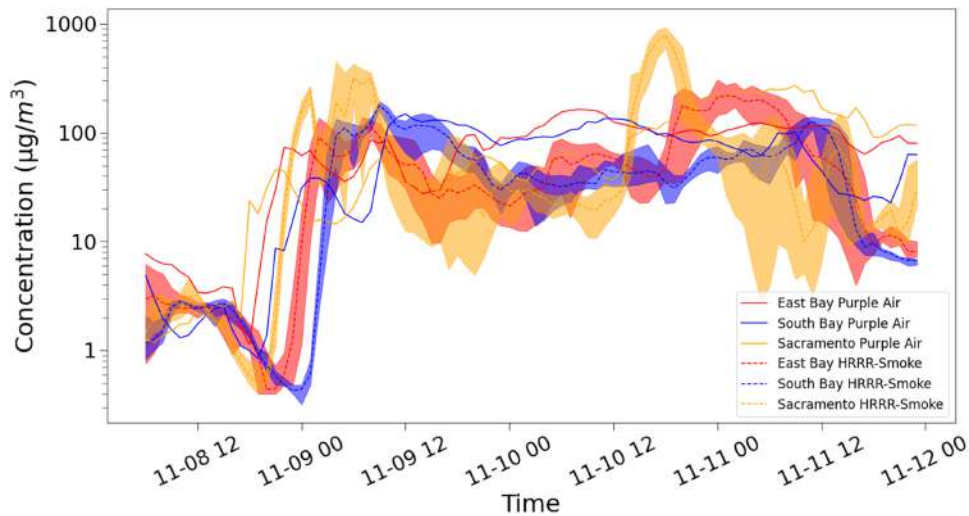
Fig. 4. Time series of PM$_{2.5}$ concentrations (μg m^{-3}) from HRRR-Smoke (dashed lines) at Sacramento, East Bay, and South Bay locations compared to averaged PurpleAir sensors (solid lines) during the initial phase of the Camp Fire event (8–12 Nov 2018). Dashed lines are the model mean over the selected areas, with shading indicating min and max values.

To examine the vertical extent of the smoke plume, Fig. 7 shows two vertical cross sections of the PM$_{2.5}$ concentration from HRRR-Smoke compared with stereoscopic satellite estimates of plume height from Carr et al. (2019). The satellite plume height retrieval has ~8-km spatial resolution and retrieves the topographic height in regions without optically thick features like clouds or dense smoke. The satellite retrieved heights track the topography of the Sierra peaks seen in the HRRR-Smoke data, with an estimated error of ±200 m (Carr et al. 2019), meaning that no dense smoke was detected in this area, in agreement with the HRRR-Smoke prediction. The HRRR-Smoke plume evolves rapidly, with changes in the smoke plume altitude occurring each hour; several time snapshots were examined and the peak plume height varied considerably near the source at 39.6°N.

Figure 7a shows results at 39.6°N latitude, near the fire source in Paradise, with the *Aqua*/MODIS and *GOES-16* joint stereo retrieval from 1855 UTC 9 November 2018 (see Fig. 31 from Carr et al. 2019), and HRRR-Smoke is shown at 0000 UTC 10 November 2018. This model time was selected as it shows the best qualitative agreement with the observed plume height during this time period; additional time slices are shown in the supplemental material. The satellite data show a rapid drop of the smoke plume height from 4 km elevation near the fire source at 126°W, to 2-km elevation on the left at 122.5°W, and this trend is largely captured by HRRR-Smoke.

Figure 7b shows a slice from 2115 UTC 10 November 2018 at 37.8°N latitude, crossing near San Francisco airport and near the site of the Oakland sounding (see Fig. 32 from Carr et al. 2019), with plume tops of about 1.2 km over the ocean and rapidly rising to a height of 2500 m over the East Bay hills (at ~122°W). HRRR-Smoke shown at 2100 UTC also shows elevated concentrations centered over the Bay Area (122.5°–122°W) with the plume top reaching 2000–2500 m in the East Bay.

Vertical profiles of HRRR-Smoke output are included in sounding profiles in the following section. The time variability of the vertical structure of the HRRR-Smoke plume is also captured at 6-h intervals in the ceilometer data shown in Fig. A2 of the appendix. The complex 3D distribution of smoke over this region is driven by the fire plume rise, transport, and boundary layer mixing. The qualitative agreement of the model forecast with the stereo-tracking satellite data shows that the model is able to simulate the dynamic processes which drive the smoke distribution. The next section shows that the model forecast the meteorological fields well.
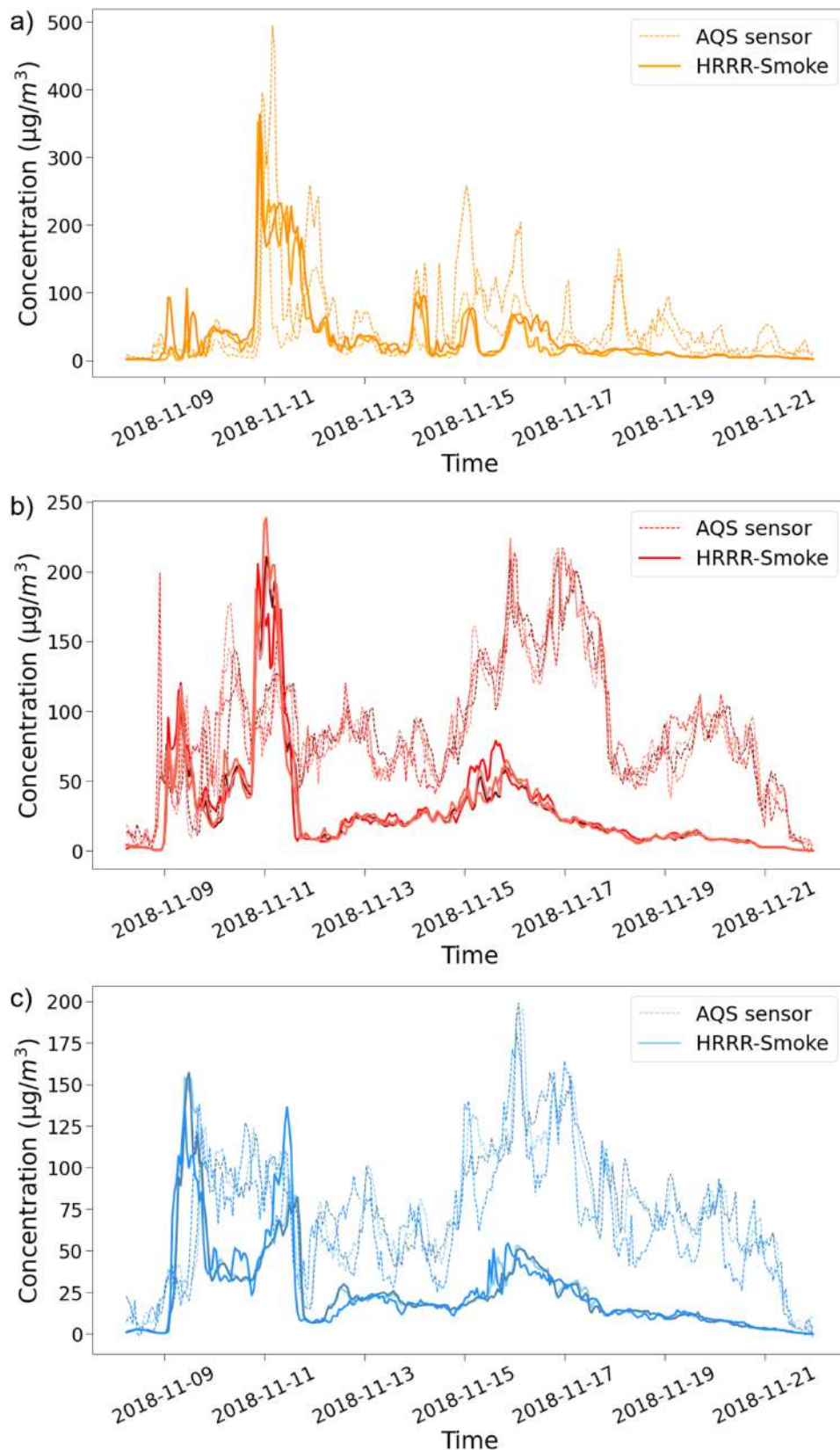
Fig. 5. Time series of PM$_{2.5}$ concentrations (μg m^{-3}) from HRRR-Smoke and AQS stations in (a) Sacramento, (b) East Bay, and (c) South Bay. Individual AQS sensors (dashed lines) and the nearest HRRR-Smoke grid point for each of the sensors (solid lines) are plotted. Note the different axis limits.
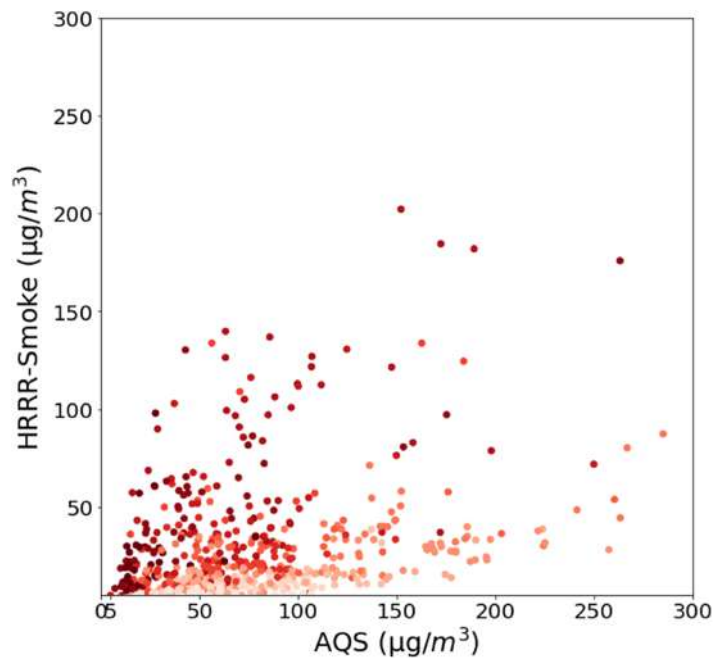
Fig. 6. Scatterplot of daily averaged PM$_{2.5}$ concentrations (μg m^{-3}) from HRRR-Smoke vs AQS sensors located in the domain shown in Fig. 2. The dot color value indicates the time since the start of the fire, with darker red colors indicating measurements during the first week, and the lighter color indicating measurements during the second week of the smoke event. Daily averages are computed using values from midnight to midnight local time.

Comparison to meteorological observations

To further explain the observed behavior of the smoke plume in observations and in the model, we examine the meteorological conditions driving the smoke event, including surface observations and vertical profiles. The Camp Fire event was characterized by an east–west surface pressure gradient causing very strong downslope winds combined with very dry conditions (very low relative humidity, 10% during the day and in the teens at night). Wind speeds were 12–14 m s^{-1}, and a 23 m s^{-1} (52 mph) gust was recorded at the Jarbo Gap site near Paradise, California, early that morning (NWS Western Region Headquarters 2020). A detailed analysis of synoptic flow conditions is found in Brewer and Clements (2020).

Time series and vertical sounding comparisons of surface temperatures, wind speed, and wind direction confirm that HRRR-Smoke matched observations quite well. Figure 8 shows the vertical sounding upwind at Reno, Nevada, indicating stable conditions at night (1200 UTC = 0400 local time) with a capping inversion near mountain crest height, winds from the East, and a very dry boundary layer, leading to the downslope windstorm that fueled the Camp Fire on the lee side of the ridge (Brewer and Clements 2020). During the day (0000 UTC = 1600 local time) a mixed layer develops with stable conditions aloft and persistent low moisture. Profiles of smoke concentration (mass density) are negligibly small in Reno, located upwind of the fire. In the Oakland soundings in Fig. 8, we see a set of layered stable regions near the ground at night and a mixed layer during the day, with winds largely from the northeast. The boundary layer is quite dry. The smoke concentration increases to over 50 μg m^{-3} at the surface on 1200 UTC 9 November. By 15–16 November, with very weak winds and very stable conditions near the ground even during the daytime, smoke concentrations in Oakland are 50 μg m^{-3} at the surface (see Fig. 5b) and have increased to more than 100 μg m^{-3} at about 1 km MSL (Fig. 9). These comparisons, in addition to the corresponding 0000 UTC comparisons shown in Figs. ES3 and ES4, demonstrate the relatively good agreement between HRRR and the observed profiles.
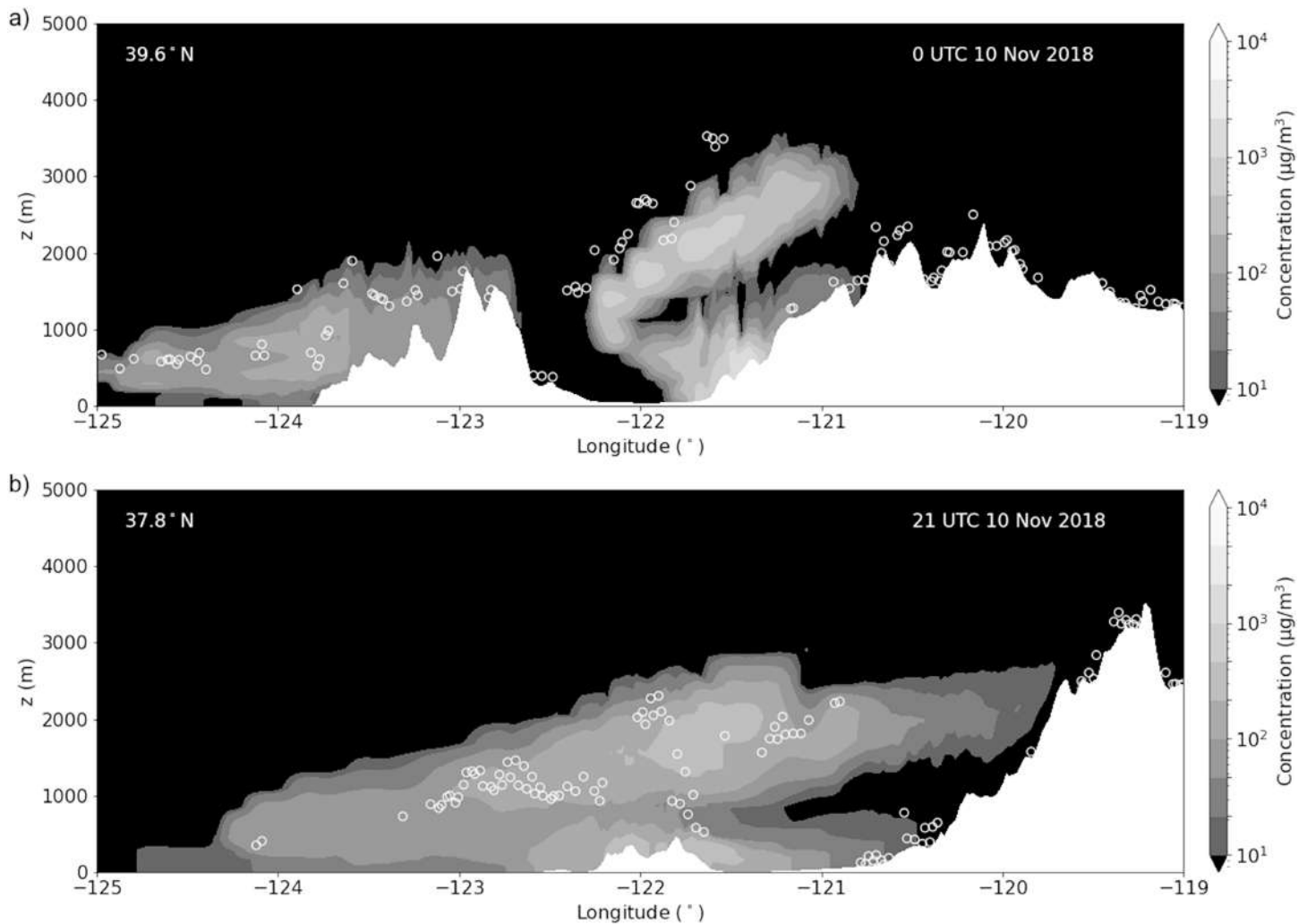
Fig. 7. Vertical cross section at (a) 39.6° and (b) 37.8°N showing contours of PM$_{2.5}$ concentrations (μg m^{-3}) from HRRR-Smoke compared to stereoscopic satellite plume height retrievals (open circles) reported as elevation (m MSL). (a) HRRR-Smoke data at 0000 UTC 10 Nov 2018 with the *Aqua*/MODIS and *GOES-16* joint stereo retrieval from 1855 UTC 9 Nov 2018. (b) HRRR-Smoke data at 2100 UTC 10 Nov 2018 with the *Aqua*/MODIS and *GOES-16* joint stereo retrieval from 2115 UTC 10 Nov 2018. Stereo plume height data are shown within ±0.025° latitude of the specified latitude. HRRR-Smoke values at this latitude are obtained via interpolation.

Figure 10 shows time series for the first few days of the Camp Fire of wind speed, wind direction, and temperature at Reno and at two stations near Paradise, namely, Jarbo Gap on the slope and Openshaw in the valley, shown in Fig. 3. Again the model shows good agreement with observations, capturing the northeast wind direction (~45°) during 0600–1200 UTC and later the increasing wind speeds at Reno upwind of the Sierras. Time series at Jarbo Gap, near the location of the fire, show the dramatic increase in winds on the downslope side of the Sierras, of 12–14 m s^{-1} from 0600 to 1200 UTC 8 November coming from the northeast. At the Openshaw station, located south of Chico in the Central Valley, winds were down valley from the north-northwest with periodic interruptions of north-northeast downslope flows from the Sierra Nevada range. Further analysis and quantification of model errors compared to observations are included in the appendix.

Satellite FRP detection challenges
The meteorological variables are captured very well by HRRR-Smoke at 3-km resolution over the complex terrain of the western United States, as seen by the foregoing discussion and
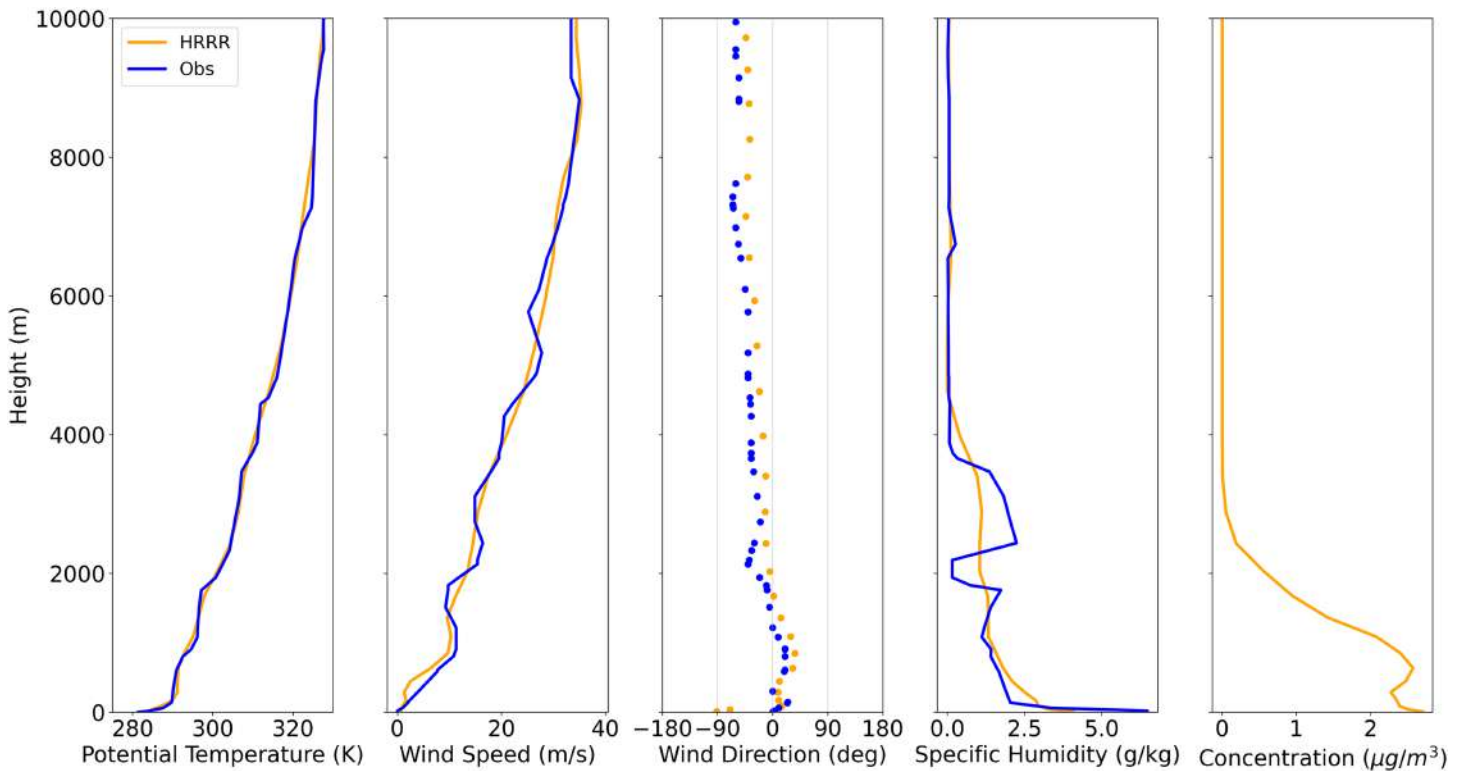
08-Nov-2018-12Z Reno
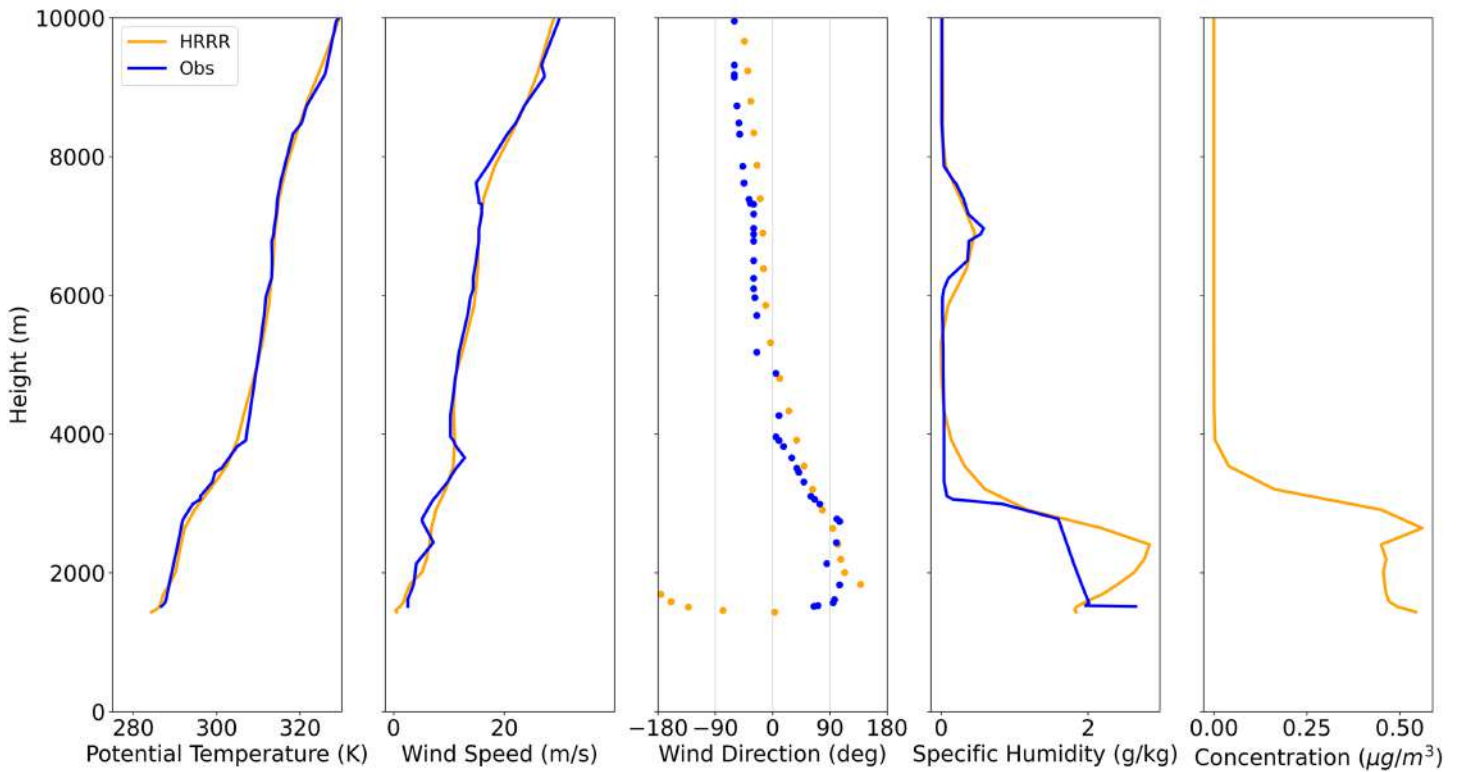
08-Nov-2018-12Z Oakland

Fig. 8. Vertical profiles of (from left to right) potential temperature, wind speed, wind direction, specific humidity, and PM$_{2.5}$ concentration (modeled only) at (top) Reno and (bottom) Oakland at 1200 UTC 8 Nov 2018 from HRRR-Smoke and from observations. 12-h HRRR is the 12-h lead-time forecast (i.e., forecast made at 0000 UTC 8 Nov 2018). Note the different axis limits.
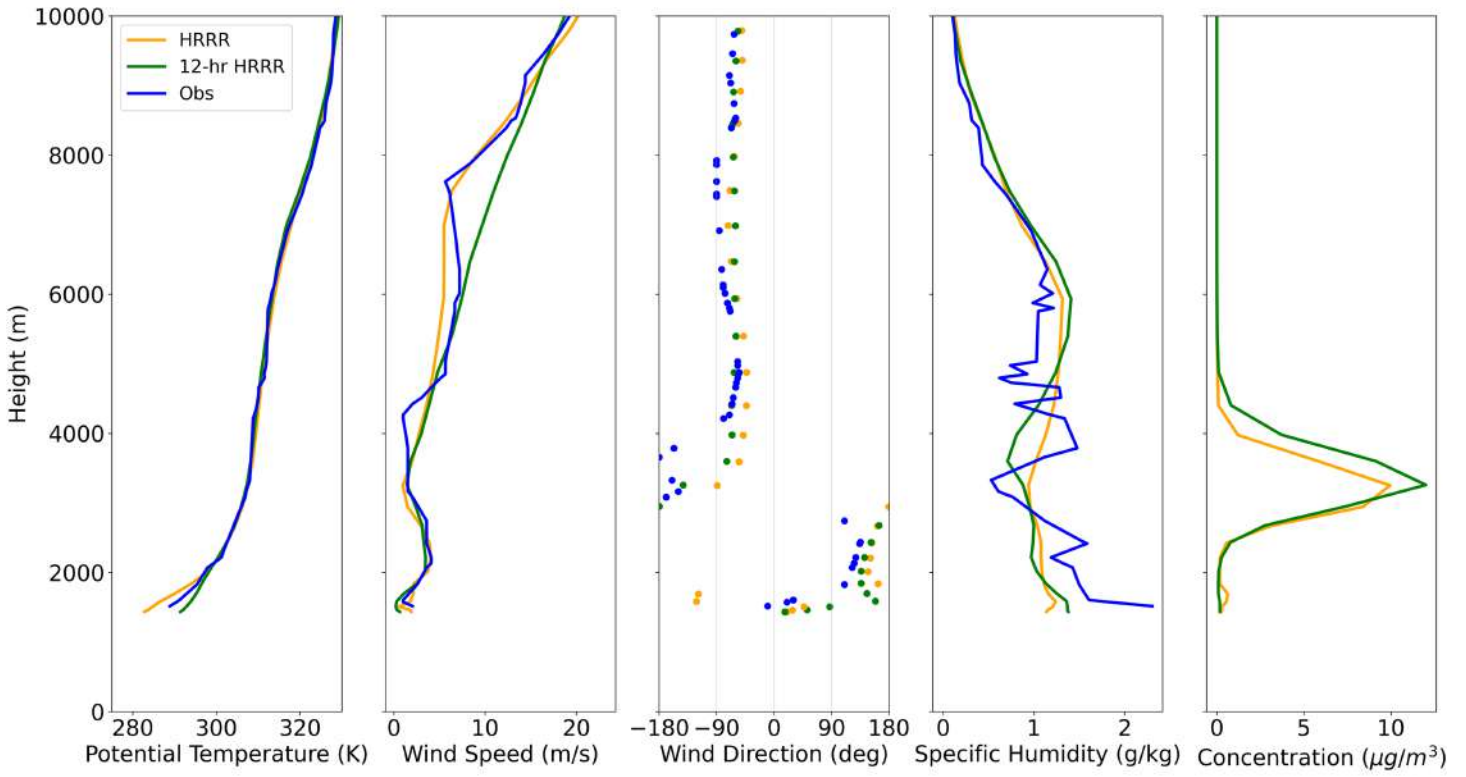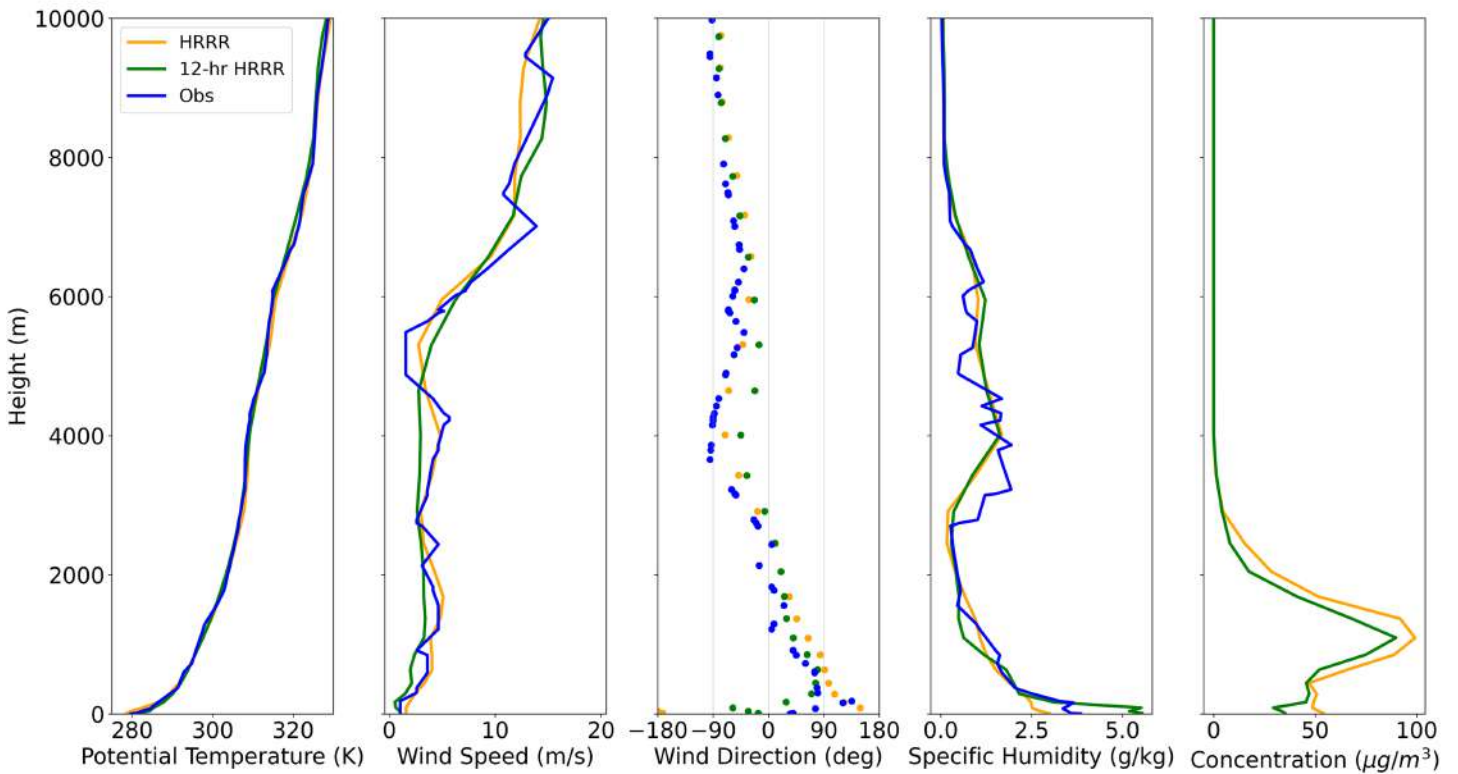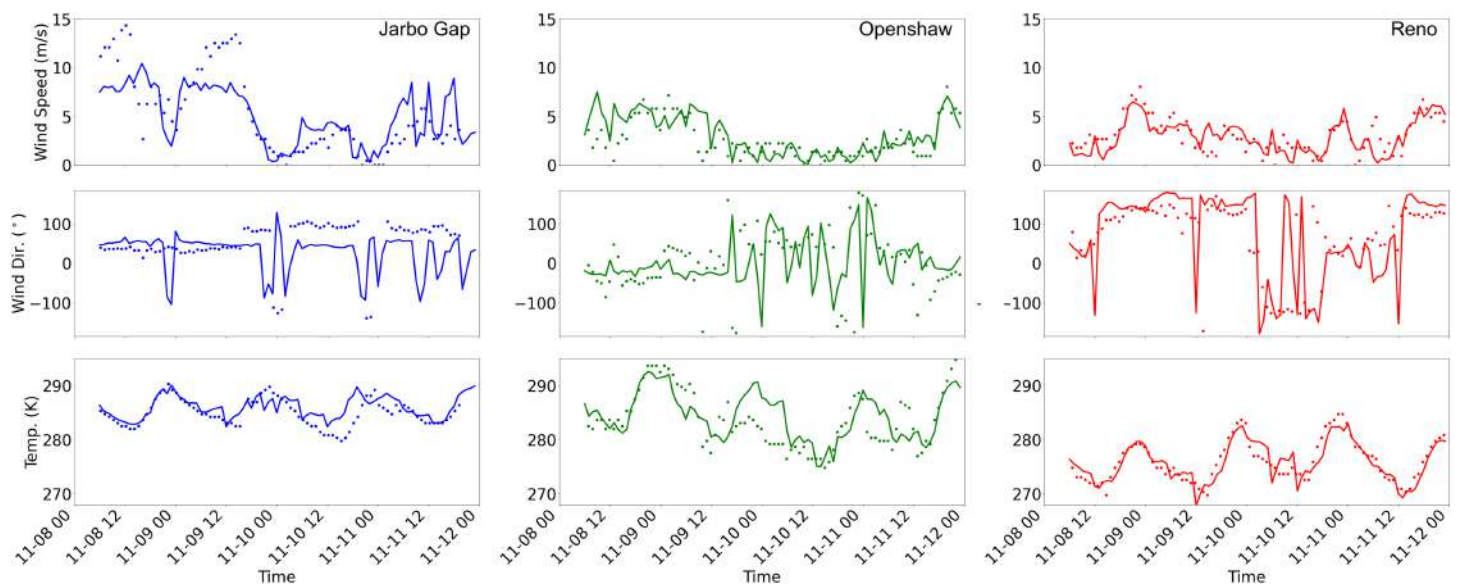
Fig. 9. As in Fig. 8, but at 1200 UTC 15 Nov 2018. 12-h HRRR is the 12-h lead-time forecast (i.e., forecast made at 0000 UTC 15 Nov 2018). Note the different axis limits.

Fig. 10. Time series of (top) wind speed, (middle) wind direction, and (bottom) temperature surface station data (dots) at (left) Jarbo Gap (blue), (center) Openshaw (green), and (right) Reno (red) compared to HRRR output at nearest grid point (solid lines).

further analysis included in the appendix. The evolution of the smoke concentration is also well represented by HRRR-Smoke, considering the complexity of the domain and the uncertainties regarding the fire detection and forecasting the fire emissions and spread. Figure 11 shows qualitative comparisons of the vertically integrated smoke and VIIRS satellite images captured in the afternoon on selected dates (a video from the model output is included in the supplemental material). Qualitative agreement is best at the beginning of the time period, and the images show remarkable similarities in the smoke plume structures, including the initial high-altitude spread of the plume on 8 November, the V-shaped structure on 9 November, the thick smoke concentrated near Paradise on 12 November, and the stagnant smoke that settles over the Central Valley and the Bay Area around 15 November. By 12 and 15 November, as seen earlier in Fig. 5, the agreement of the HRRR-Smoke $PM_{2.5}$ concentrations with observations has decreased, with the model showing a significantly lower $PM_{2.5}$ concentration spread over California.

HRRR-Smoke represents wildfires by surface fluxes prescribed by satellite detection of FRP (Ahmadov et al. 2017). A climatological diurnal cycle is used to represent hourly variability of the biomass-burning emissions in HRRR-Smoke. A plume rise model also plays a vital role in injecting smoke directly into the free troposphere (Freitas et al. 2007, 2010). Figure 12 shows time series of the FRP data ingested from polar-orbiting satellites during the Camp Fire event, showing the dramatic decrease in FRP after 8 November. (Note that Fig. 5 shows very high smoke concentrations measured even during times when the FRP detected was low.) The FRP is retrieved for pixels flagged as *fire* in the VIIRS I-band and MODIS fire products (Li et al. 2018). The model ingests the FRP data from 2 VIIRS (*NOAA-20* and *Suomi NPP*) and 2 MODIS (*Terra* and *Aqua*) sensors in real time. Each of these sensors on polar-orbiting satellites can detect fires two or more times per day in the midlatitudes unless the satellite view is blocked by clouds or dense smoke. The daily sequence of daytime *Suomi NPP* images shows a good delineation of the fire front of the Camp Fire event between 8 and 12 November (see Fig. ES5 in the supplemental material). On 13 November, however, no daytime detections were reported by the algorithm due to persistent (though not totally opaque) cloud cover. *NOAA-20* and *Terra/Aqua* FRP data (not shown) follow similar patterns. Because the fire intensities are usually high during daytime, such omission of the satellite FRP data entirely during the daytime leads to very low biomass burning flux estimates ingested into the model. The HRRR-Smoke model cycles smoke between subsequent forecasts, therefore the following forecast cycles
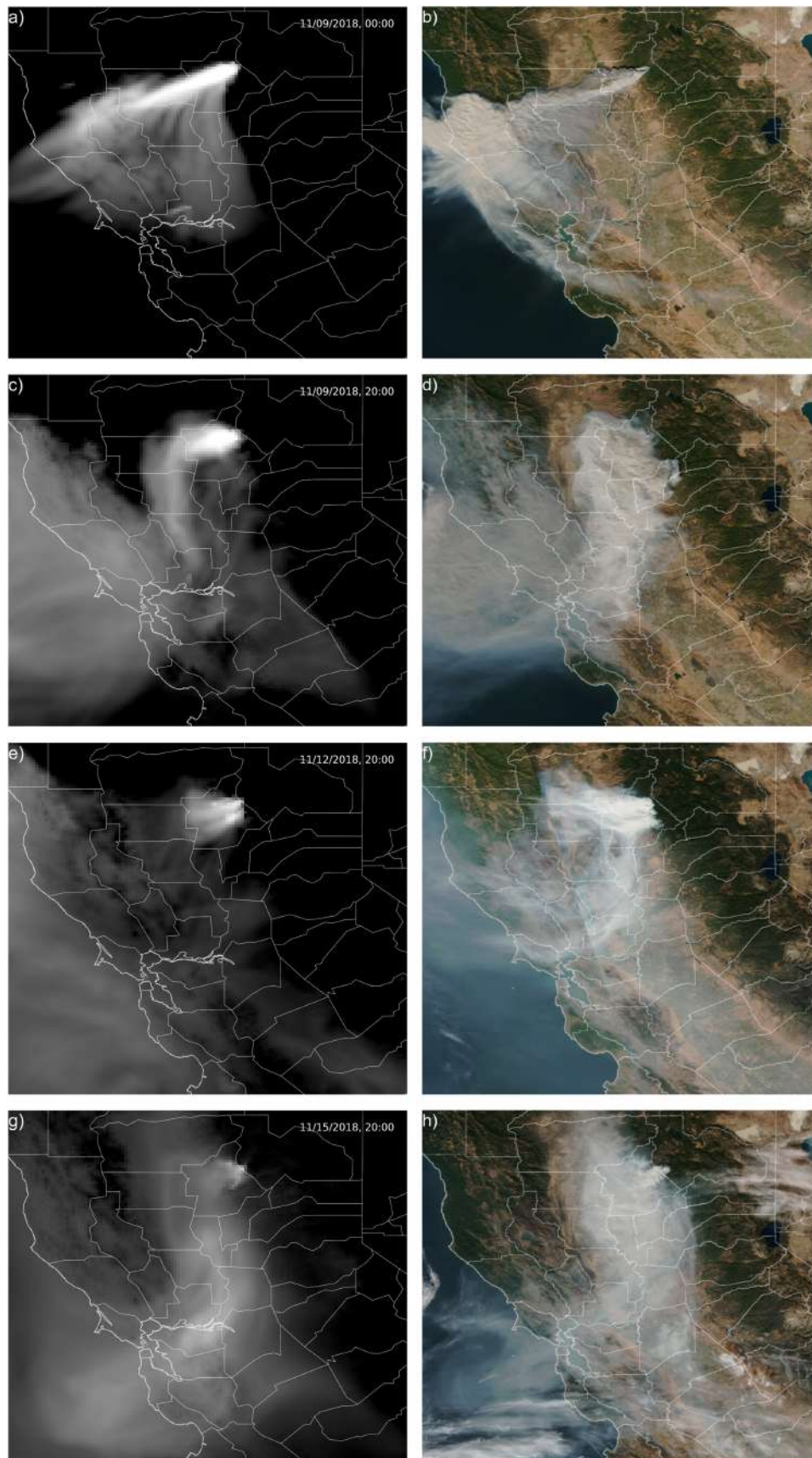
Fig. 11. (left) HRRR-Smoke vertically integrated smoke compared to (right) *Suomi NPP* visible images. Dates are (a),(b) 8, (c),(d) 9, (e),(f) 12, (g),(h) 15 Nov 2018. HRRR-Smoke output is shown at 2000 UTC, which roughly matches the satellite crossover times, except for the first HRRR-Smoke image, which is shown at 0000 UTC 9 Nov to account for the delay in fire ignition in the model.
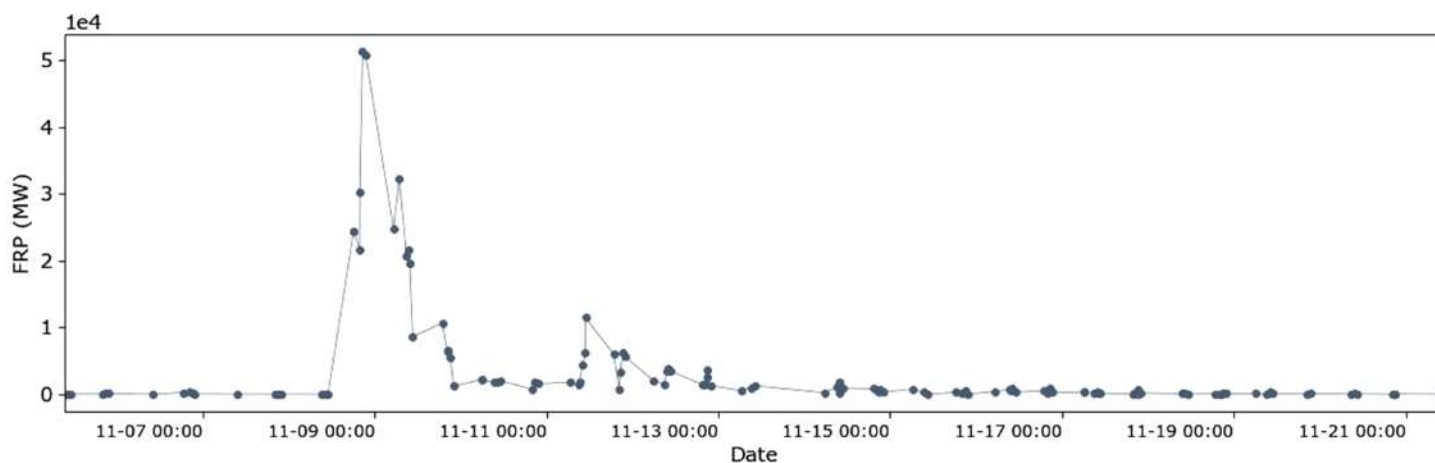
Fig. 12. Time series of the instantaneous fire radiative power for the Camp Fire, as detected by the two VIIRS and two MODIS instruments, spatially aggregated for the entire Camp Fire area.

are also impacted by the daytime FRP omission on 13 November. From 14 to 20 November, daytime detections were reported again by the algorithm, but with the omission of some areas of active burning. Nighttime detections (not shown) provided more complete spatial coverage of the areas of active burning throughout the entire time period of 8–20 November analyzed. The loss of detection of active burning during the daytime in this instance is likely the result of an increase in near-infrared reflectance from heavy smoke, which can trigger various internal nonfire tests within the detection algorithm which exclude the pixel from further consideration as possibly containing a fire. In contrast, very windy conditions tend to push thick smoke away from the path of radiance between the fire and the satellite sensor and hence allow for a more unobstructed observation of the fire; this increases the likelihood of detection and FRP retrieval. Such windy conditions were observed in particular on 8–9 and 12 November, with relative drops in FRP recorded in between (see Fig. 12).

Conclusions and future work

With wildfires now creating large-scale smoke events which regularly affect large populations in the western United States, the need for a robust wildfire smoke prediction model like HRRR-Smoke is clear. The 2018 Camp Fire event allowed detailed comparison of $PM_{2.5}$ from the wildfire smoke with AQS and PurpleAir observations to validate HRRR-Smoke because of the very low background $PM_{2.5}$ levels during that time period. HRRR-Smoke captured the meteorology very well and hence captured the qualitative spatial structure of the smoke (Fig. 11) over Northern California, particularly during the first few days of the Camp Fire event. Comparisons with satellite stereo plume height data were used for the first time, to the authors' knowledge, to verify the 3D plume transport in the model. The HRRR-Smoke model also includes smoke feedback on meteorology and captured the stagnation event during the second week of the event. Comparisons to new dense surface station networks from PurpleAir and AQS sites allowed spatial patterns in smoke evolution to be verified.

One of the limitations of the HRRR-Smoke model is its reliance on relatively infrequent and possibly degraded observations of FRP derived from satellite observations. The satellite FRP was underestimated overall during the second half of the smoke event. The VIIRS data at 375-m resolution is the highest resolution instrument for satellite fire detection, thus with respect to sensitivity and spatial fidelity VIIRS imagery will often be the source of choice for FRP data. At present only data from polar-orbiting satellites are employed in the model, reducing sampling frequency to a few daytime and a few nighttime observations. Inclusion of data from the geostationary GOES-R platforms will significantly improve temporal

coverage (O'Neill and Raffuse 2021). Another approach to account for FRP errors would be to use source inversion modeling based on the dense surface station networks, to adjust the smoke emissions from the fires (see, e.g., Kim et al. 2020). Additionally, data assimilation can be used to compensate for errors in the source terms. For instance, assimilating the surface $PM_{2.5}$ measurements in conjunction with the satellite aerosol optical depth data into the smoke forecasting models can improve the accuracy of the smoke forecasts in the future (Saide et al. 2014). Emerging comparisons with ceilometer data will also allow better evaluation of the vertical structure of wildfire smoke plumes (Huff et al. 2021; Li et al. 2021), as will further model comparisons to satellite stereoscopic plume height observations (Carr et al. 2019).

HRRR-Smoke is becoming an essential tool for providing real-time operational support for weather and air quality forecasters. Because the model includes radiation feedback from the smoke, which affects surface temperatures, it is able to capture smoke-induced events like the "orange skies" seen in California lightning complex fires of August 2020 (NESDIS 2021). HRRR-Smoke currently restarts hourly, which allows it to ingest new satellite detection data at a very high frequency compared to other air quality models. Further validation and improvement of the model are needed to enable more accurate prediction of wildfire or prescribed burn smoke events for community health and safety. Ultimately, modeling and sensor networks can be combined to provide robust nowcasts and forecasts for poor air quality events due to wildfire smoke.

Data availability statement. The model data that support the findings of this study are available from the corresponding author upon reasonable request and/or from the HRRR-Smoke website (https://rapidrefresh.noaa.gov/hrrr/HRRRsmoke/). The meteorological and air quality data that support the findings of this study are publicly available from PurpleAir (https://api.purpleair.com), AirData (https://www.epa.gov/outdoor-air-quality-data), NOAA RAWS (https://wrcc.dri.edu/wraws/ccaF.html), and satellite images from NOAA NESDIS JSTAR Mapper (www.star.nesdis.noaa.gov/jpss/mapper/) websites.

Appendix: Model and sensors
Model. The HRRR is an hourly data assimilation and weather forecast system. There are 50 vertical levels, and the model top is at 15 hPa. The center of the lowest model level is ~8 m AGL at sea level. The model is run over the CONUS domain (1800 × 1060 grid points). The HRRR uses the MYNN PBL scheme (Olson 2019), the RUC land surface model (Smirnova et al. 2016), RRTMG shortwave and longwave radiation schemes (Iacono et al. 2008), and the Thompson microphysics scheme (Thompson and Eidhammer 2014). A smoke tracer, a plume rise parameterization (Freitas et al. 2007, 2010), and fire radiative power processing (Ahmadov et al. 2017) were added to create HRRR-Smoke. HRRR-smoke includes only a single smoke tracer, with no gas or aerosol chemistry, although wet and dry removal are included. A climatological diurnal cycle is used to represent hourly variability of the biomass burning emissions in HRRR-Smoke. HRRR-Smoke ingests FRP from the polar-orbiting satellite data. Each simulation uses FRP detections from the 24 h prior to initialization time. The plume rise parameterization describes plume rise due to the fire heat flux. Some details of the HRRR configuration differ between what was run in real time in 2018 versus what was run retrospectively (in forecast mode) for this study. The retrospective simulations used for this study carried out hybrid ensemble 3DVar data assimilation for meteorology (Hu et al. 2017) based
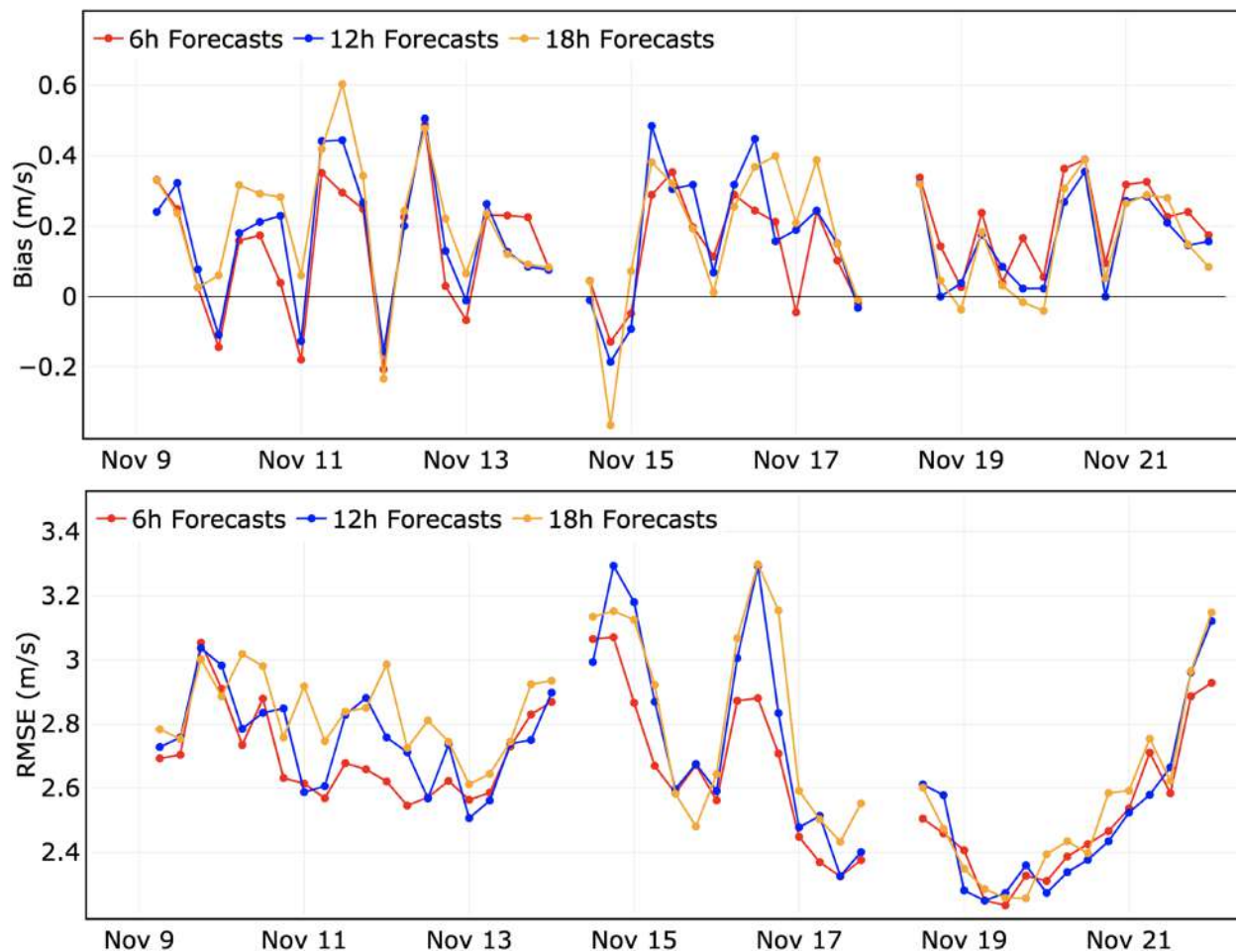
Fig. A1. (top) Bias and (bottom) RMSE plots for 10-m wind speed from 9 to 22 Nov 2018 comparing HRRR-Smoke output with all METAR surface stations in the northwestern continental United States.

on the community Gridpoint Statistical Interpolation (GSI; Kleist et al. 2009). Background error covariances are a blend of ensemble covariances from the 80-member Global Data Assimilation System (GDAS) ensemble and static covariances (Wang 2010). Many conventional observations are assimilated hourly in a manner analogous to the 13-km Rapid Refresh (RAP) system (Benjamin et al. 2016); HRRR does not assimilate any smoke or chemistry observations. The background for the HRRR data assimilation comes from a 1-h "preforecast" in which 15-min radar reflectivity observations are assimilated. The preforecast is initialized from a downscaled RAP 0-h analysis; boundary conditions for both the preforecast and full forecast come from the RAP. The model component of the HRRR is based on WRF-ARW (Powers et al. 2017), with advanced physics parameterizations (Benjamin et al. 2016). For the retrospective analysis done here, HRRR was rerun at 6-h forecast intervals to conserve computational resources (compared to hourly restarts done operationally). Frequent restarts are important to capture the onset of the fire, where MODIS *Terra* detected it at 1810 UTC 8 November (1010 local time), and HRRR ingested it. The retrospective forecast was done using VIIRS I-band (375-m resolution) as input as opposed to M-band (750-m resolution), which was used in the real-time modeling. Simulations were initialized at 0000, 0600, 1200, and 1800 UTC, and forecasts extended to 24-h lead time.

Figure A1 shows time series of model 10-m wind bias and RMSE compared to all METAR surface stations in the northwest continental United States during the entire duration of the Camp Fire. Absolute bias values are generally below 0.5 m s^{-1}, and RMSE generally stays below 3 m s^{-1} except during 14–16 November when the peak errors of 3.3 m s^{-1} occur during the daytime for the 12- and 18-h forecasts; the timing of these peak errors corresponds
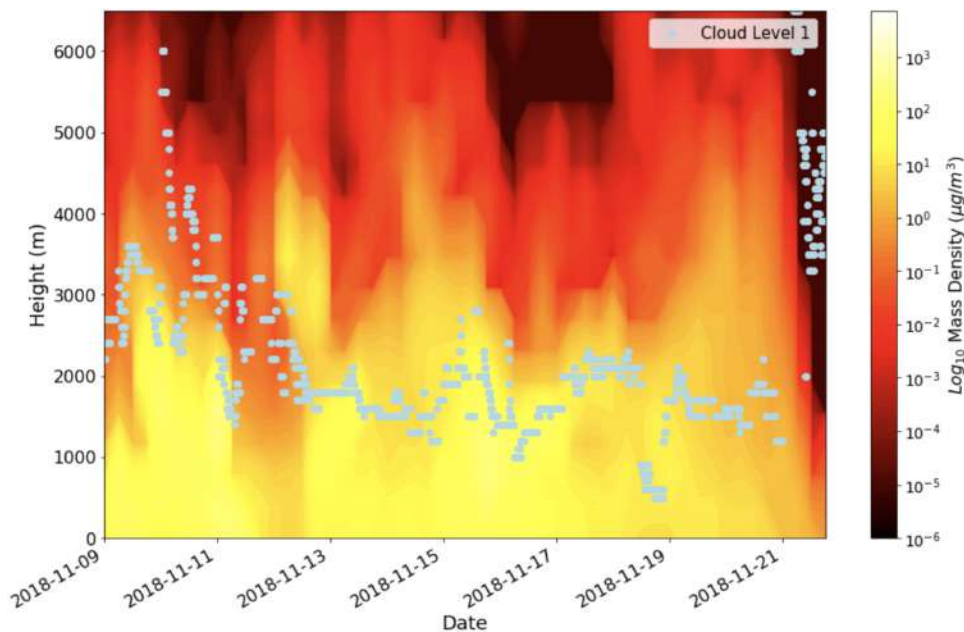
Fig. A2. Time–height contours of HRRR-Smoke PM$_{2.5}$ concentration overlaid with the first cloud level from Oakland airport METAR ceilometer data (dots).

to the passage of upper-level shortwave troughs across British Columbia. The 6-h forecast performs considerably better throughout the entire period, both in terms of bias and RMSE, illustrating the benefit of frequent data assimilation. Similar statistics (not shown) are found in comparisons to upper-air observations (radiosondes). These statistics, combined with detailed comparisons at specific locations (as seen in Figs. 8–10) confirm that the meteorological representation from HRRR-Smoke was overall in good agreement with surface and upper-air observations.

A final additional comparison of model output and observations is offered in Fig. A2, which compares ceilometer observations with vertical profiles of smoke from HRRR-Smoke. We can see elevated layers of smoke that sometimes correspond with ceilometer cloud levels. The ceilometer readings are from Automated Surface Observing System (ASOS) stations, which are collected from ceilometers at airports across the United States. As shown in Fig. A2, the ceilometer data are not the raw output, but rather passed through an algorithm to obtain several cloud levels. The cloud levels are intended to represent the base of cloud banks in the upper atmosphere that cause backscattering of the ceilometer beam. In Fig. A2, the cloud level with the lowest altitude is plotted as "Cloud Level 1." In cases where fog conditions mask the base of a cloud, readings from the ceilometer are then interpreted as restricted vertical visibility (NOAA 1998). The ASOS algorithm is calibrated to calculate the vertical visibility for foggy conditions, and the variation in the cloud level data for the smoke suggests that it may be treating the smoke as a near-surface fog layer, likely depending on the near-surface density of smoke. Although not available at these sites, raw ceilometer data could provide a detailed characterization of smoke plumes aloft and near the surface. Wu et al. (2018) showed that raw ceilometer data provided a clear picture of the smoke plume from Canadian wildfires in 2016. These emerging comparisons with ceilometer networks will allow better evaluation of the vertical structure of wildfire smoke plumes in the future (National Research Council 2009; Huff et al. 2021).

Sensors. The PurpleAir network consists of low-cost PM$_{2.5}$ sensors, predominantly marketed for monitoring local air quality near homes or work places. The low cost of the sensors has increased their rate of adoption and created a relatively dense real-time air quality sensor

network in and around the populated areas of California. Direct comparisons with groups of PurpleAir sensors in the Bay Area were made in three areas of interest with adequate density of PurpleAir sensors: East Bay, South Bay, and Sacramento. High sensor densities in these three areas increase the robustness of the comparison with the HRRR-Smoke model.

Publicly maintained low-cost air sensors are subject to more errors than the AQS sensors maintained by air quality agencies, but can provide detailed information about local spatial variations in $PM_{2.5}$. Common issues with the low-cost sensors include data gaps, extremely high or low values, and some loss of accuracy in high-relative-humidity and high-coarse-particle-concentration conditions (Stavroulas et al. 2020). To minimize any such errors, we focused on areas with dense sensor networks to ensure that individual sensors could be compared to the aggregate network to remove outliers. Further, any sensors with gaps in data over the time period of interest were removed. Finally, the two separate channels on the PurpleAir sensors were compared to determine if the sensor had any technical issues causing internal discrepancies.

PurpleAir sensors are known to overall overpredict PM values compared to Federal Reference Method (FRM) data. Recently, a new EPA correction formula (Barkjohn et al. 2021) has become available in the lower-left drop-down menu on the PurpleAir website. This EPA correction formula accounts for variability in relative humidity across the United States. The formula provides a linear best-fit adjustment factor and an intercept based on U.S.-wide data, which overall is based on lower-concentration data (non-wildfire data). The EPA correction is very similar to the 0.48 PurpleAir adjustment factor determined by Delp and Singer (2020) for the Camp Fire. Both approaches give similar results within 5% during wildfire events. Because the Delp and Singer (2020) data were adjusted specifically for the 2018 Camp Fire, we have selected to use the simpler 0.48 correction factor in all presentations of the PurpleAir data. The reader is referred to Delp and Singer (2020) for further detailed analysis.

Using these constraints to filter the PurpleAir data, the averaged HRRR-Smoke data could be compared to the averaged PurpleAir data from sensors within each area (Fig. 4). While AQS sensors provide more reliable information, the density of the AQS network was not high enough to generate a fair comparison between AQS sensors and the average HRRR value. As a result, we opted instead to compare individual AQS sensors with their closest gridded HRRR data points (Fig. 5).

References

Ahmadov, R., and Coauthors, 2017: Using VIIRS fire radiative power data to simulate biomass burning emissions, plume rise and smoke transport in a real-time air quality modeling system. *2017 IEEE Int. Geoscience and Remote Sensing Symp.*, Fort Worth, TX, Institute of Electrical and Electronics Engineers, 2806–2808, https://doi.org/10.1109/IGARSS.2017.8127581.

Balmes, J. R., 2020: The changing nature of wildfires: Impacts on the health of the public. *Clin. Chest Med.*, **41**, 771–776, https://doi.org/10.1016/j.ccm.2020.08.006.

Ban, Y., P. Zhang, A. Nascetti, A. R. Bevington, and M. A. Wulder, 2020: Near real-time wildfire progression monitoring with Sentinel-1 SAR time series and deep learning. *Sci. Rep.*, **10**, 1322, https://doi.org/10.1038/s41598-019-56967-x.

Barkjohn, K. K., B. Gantt, and A. L. Clements, 2021: Development and application of a United States-wide correction for PM2.5 data collected with the PurpleAir sensor. *Atmos. Meas. Tech.*, **14**, 4617–4637, https://doi.org/10.5194/amt-14-4617-2021.

Benjamin, S. G., and Coauthors, 2016: A North American hourly assimilation and model forecast cycle: The rapid refresh. *Mon. Wea. Rev.*, **144**, 1669–1694, https://doi.org/10.1175/MWR-D-15-0242.1.

——, and Coauthors, 2021: Stratiform cloud-hydrometeor assimilation for HRRR and RAP model short-range weather prediction. *Mon. Wea. Rev.*, **149**, 2673–2694, https://doi.org/10.1175/MWR-D-20-0319.1.

Brewer, M. J., and C. B. Clements, 2020: The 2018 Camp Fire: Meteorological analysis using in situ observations and numerical simulations. *Atmosphere*, **11**, 47, https://doi.org/10.3390/atmos11010047.

Burke, M., A. Driscoll, S. Heft-Neal, J. Xue, J. Burney, and M. Wara, 2021: The changing risk and burden of wildfire in the United States. *Proc. Natl. Acad. Sci. USA*, **118**, e2011048118, https://doi.org/10.1073/pnas.2011048118.

Carr, J. L., D. L. Wu, R. E. Wolfe, H. Madani, G. G. Lin, and B. Tan, 2019: Joint 3D-wind retrievals with stereoscopic views from MODIS and GOES. *Remote Sens.*, **11**, 2100, https://doi.org/10.3390/rs11182100.

Delp, W. W., and B. C. Singer, 2020: Wildfire smoke adjustment factors for low-cost and professional PM2.5 monitors with optical sensors. *Sensors*, **20**, 3683, https://doi.org/10.3390/s20133683.

Freitas, S. R., and Coauthors, 2007: Including the sub-grid scale plume rise of vegetation fires in low resolution atmospheric transport models. *Atmos. Chem. Phys.*, **7**, 3385–3398, https://doi.org/10.5194/acp-7-3385-2007.

——, K. M. Longo, J. Trentmann, and D. Latham, 2010: Technical note: Sensitivity of 1-D smoke plume rise models to the inclusion of environmental wind drag. *Atmos. Chem. Phys.*, **10**, 585–594, https://doi.org/10.5194/acp-10-585-2010.

Grell, G., S. R. Freitas, M. Stuefer, and J. Fast, 2011: Inclusion of biomass burning in WRF-Chem: Impact of wildfires on weather forecasts. *Atmos. Chem. Phys.*, **11**, 5289–5303, https://doi.org/10.5194/acp-11-5289-2011.

Gupta, P., and Coauthors, 2018: Impact of California fires on local and regional air quality: The role of a low-cost sensor network and satellite observations. *GeoHealth*, **2**, 172–181, https://doi.org/10.1029/2018GH000136.

Holm, S. M., M. D. Miller, and J. R. Balmes, 2021: Health effects of wildfire smoke in children and public health tools: A narrative review. *J. Exposure Sci. Environ. Epidemiol.*, **31**, 1–20, https://doi.org/10.1038/s41370-020-00267-4.

Hu, M., S. G. Benjamin, T. T. Ladwig, D. C. Dowell, S. S. Weygandt, C. R. Alexander, and J. S. Whitaker, 2017: GSI three-dimensional ensemble–variational hybrid data assimilation using a global ensemble for the regional rapid refresh model. *Mon. Wea. Rev.*, **145**, 4205–4225, https://doi.org/10.1175/MWR-D-16-0418.1.

Huff, A. K., S. Kondragunta, H. Zhang, I. Laszlo, M. Zhou, V. Caicedo, R. Delgado, and R. Levy, 2021: Tracking smoke from a prescribed fire and its impacts on local air quality using temporally resolved GOES-16 ABI aerosol optical depth (AOD). *J. Atmos. Oceanic Technol.*, **38**, 963–976, https://doi.org/10.1175/JTECH-D-20-0162.1.

Iacono, M. J., J. S. Delamere, E. J. Mlawer, M. W. Shephard, S. A. Clough, and W. D. Collins, 2008: Radiative forcing by long-lived greenhouse gases: Calculations with the AER radiative transfer models. *J. Geophys. Res.*, **113**, D13103, https://doi.org/10.1029/2008JD009944.

James, E. P., and Coauthors, 2019: Rapidly-updating high-resolution predictions of smoke, visibility, and smoke-weather interactions using satellite fire products within the Rapid Refresh and High-Resolution Rapid Refresh Coupled with smoke (RAP/HRRR-smoke). Phoenix, AZ, Amer. Meteor. Soc., 4B.3, https://ams.confex.com/ams/2019Annual/meetingapp.cgi/Paper/353068.

Kim, H. C., T. Chai, A. Stein, and S. Kondragunta, 2020: Inverse modeling of fire emissions constrained by smoke plume transport using HYSPLIT dispersion model and geostationary satellite observations. *Atmos. Chem. Phys.*, **20**, 10259–10277, https://doi.org/10.5194/acp-20-10259-2020.

Kleist, D. T., D. F. Parrish, J. C. Derber, R. Treadon, W.-S. Wu, and S. Lord, 2009: Introduction of the GSI into the NCEP global data assimilation system. *Wea. Forecasting*, **24**, 1691–1705, https://doi.org/10.1175/2009WAF2222201.1.

Knobel, L., 2018: Unhealthy air quality caused by Camp Fire persists in Berkeley. *Berkelyside*, 12 November, www.berkeleyside.com/2018/11/12/unhealthy-air-quality-caused-by-camp-fire-persists-in-berkeley.

Li, D., Y. Wu, B. Gross, and F. Moshary, 2021: Capabilities of an automatic lidar ceilometer to retrieve aerosol characteristics within the planetary boundary layer. *Remote Sens.*, **13**, 3626, https://doi.org/10.3390/rs13183626.

Li, F., X. Zhang, S. Kondragunta, and I. Csiszar, 2018: Comparison of fire radiative power estimates from VIIRS and MODIS observations. *J. Geophys. Res. Atmos.*, **123**, 4545–4563, https://doi.org/10.1029/2017JD027823.

Li, Y., and Coauthors, 2020: Ensemble PM2.5 forecasting during the 2018 Camp Fire event using the HYSPLIT transport and dispersion model. *J. Geophys. Res. Atmos.*, **125**, e2020JD032768, https://doi.org/10.1029/2020JD032768.

Liu, J. C., and Coauthors, 2017: Wildfire-specific fine particulate matter and risk of hospital admissions in urban and rural counties. *Epidemiology*, **28**, 77–85, https://doi.org/10.1097/EDE.0000000000000556.

Mass, C. F., and D. Ovens, 2021: The synoptic and mesoscale evolution accompanying the 2018 camp fire of Northern California. *Bull. Amer. Meteor. Soc.*, **102**, E168–E192, https://doi.org/10.1175/BAMS-D-20-0124.1.

Miller, R. K., C. B. Field, and K. J. Mach, 2020: Barriers and enablers for prescribed burns for wildfire management in California. *Nat. Sustainability*, **3**, 101–109, https://doi.org/10.1038/s41893-019-0451-7.

National Research Council, 2009: *Observing Weather and Climate from the Ground Up: A Nationwide Network of Networks.* The National Academies Press, 250 pp.

NESDIS, 2021: A model that predicts the spread of wildfire smoke becomes operational. NOAA National Environmental Satellite, Data, and Information Service (NESDIS), www.nesdis.noaa.gov/content/model-predicts-spread-wildfire-smoke-becomes-operational.

NOAA, 1998: Automated Surface Observing System (ASOS) user's guide. NOAA Doc., 74 pp., www.weather.gov/media/asos/aum-toc.pdf.

NWS Western Region Headquarters, 2020: November 2018 Camp Fire. NOAA Service Assessment, 38 pp., www.weather.gov/media/publications/assessments/sa1162SignedReport.pdf.

O'Neill, S., and S. Raffuse, 2021: Advances in satellite data for wildfire smoke forecasting. *Eos, Trans. Amer. Geophys. Union*, **102**, https://doi.org/10.1029/2021EO155076.

Olson, J. B., 2019: A description of the MYNN-EDMF scheme and the coupling to other components in WRF–ARW. NOAA Tech. Memo. OAR GSD-61, 42 pp., https://doi.org/10.25923/N9WM-BE49.

Palinkas, L. A., 2020: *The California wildfires. Global Climate Change, Population Displacement, and Public Health: The Next Wave of Migration*, L. A. Palinkas, Ed., Springer International Publishing, 53–67, https://doi.org/10.1007/978-3-030-41890-8_4.

Powers, J. G., and Coauthors, 2017: The weather research and forecasting model: Overview, system efforts, and future directions. *Bull. Amer. Meteor. Soc.*, **98**, 1717–1737, https://doi.org/10.1175/BAMS-D-15-00308.1.

Reid, C. E., M. J. Barlage, F. H. Johnston, M. Jerrett, J. R. Balmes, and C. T. Elliott, 2016: Critical review of health impacts of wildfire smoke exposure. *Environ. Health Perspect.*, **124**, 1334–1343, https://doi.org/10.1289/ehp.1409277.

Rooney, B., Y. Wang, J. H. Jiang, B. Zhao, Z.-C. Zeng, and J. H. Seinfeld, 2020: Air quality impact of the Northern California Camp Fire of November 2018. *Atmos. Chem. Phys.*, **20**, 14 597–14 616, https://doi.org/10.5194/acp-20-14597-2020.

Saide, P. E., J. Kim, C. H. Song, M. Choi, Y. Cheng, and G. R. Carmichael, 2014: Assimilation of next generation geostationary aerosol optical depth retrievals to improve air quality simulations. *Geophys. Res. Lett.*, **41**, 9188–9196, https://doi.org/10.1002/2014GL062089.

Smirnova, T. G., J. M. Brown, S. G. Benjamin, and J. S. Kenyon, 2016: Modifications to the Rapid Update Cycle Land Surface Model (RUC LSM) available in the Weather Research and Forecasting (WRF) Model. *Mon. Wea. Rev.*, **144**, 1851–1865, https://doi.org/10.1175/MWR-D-15-0198.1.

Stavroulas, I., and Coauthors, 2020: Field evaluation of low-cost PM sensors (Purple Air PA-II) under variable urban air quality conditions, in Greece. *Atmosphere*, **11**, 926, https://doi.org/10.3390/atmos11090926.

Thompson, G., and T. Eidhammer, 2014: A study of aerosol impacts on clouds and precipitation development in a large winter cyclone. *J. Atmos. Sci.*, **71**, 3636–3658, https://doi.org/10.1175/JAS-D-13-0305.1.

Wang, X., 2010: Incorporating ensemble covariance in the gridpoint statistical interpolation variational minimization: A mathematical framework. *Mon. Wea. Rev.*, **138**, 2990–2995, https://doi.org/10.1175/2010MWR3245.1.

Wettstein, Z. S., S. Hoshiko, J. Fahimi, R. J. Harrison, W. E. Cascio, and A. G. Rappold, 2018: Cardiovascular and cerebrovascular emergency department visits associated with wildfire smoke exposure in California in 2015. *J. Amer. Heart Assoc.*, **7**, e007492, https://doi.org/10.1161/JAHA.117.007492.

Wu, Y., W. Peña, B. Gross, and F. Moshary, 2018: Wildfire smoke transport and impact on air quality observed by a multi-wavelength elastic-raman lidar and ceilometer in New York city. *EPJ Web Conf.*, **176**, 05044, https://doi.org/10.1051/epjconf/201817605044.

Ye, X., and Coauthors, 2021: Evaluation and intercomparison of wildfire smoke forecasts from multiple modeling systems for the 2019 Williams Flats fire. *Atmos. Chem. Phys.*, **21**, 14 427–14 469, https://doi.org/10.5194/acp-21-14427-2021.